An Elasto-visco-plastic Model of Cell Aggregates

L. Preziosi
Department of Mathematics – Politecnico di Torino
Corso Duca degli Abruzzi 24, 10129 Torino, Italy
preziosi@polito.it

D. Ambrosi
MOX-Dipartimento di Matematica, Politecnico di Milano,
Piazza Leonardo da Vinci 32, 20131 Milano, Italy

C. Verdier
Laboratoire de Spectrométrie Physique - UMR 5588
CNRS and Université Grenoble I
140 avenue de la Physique, BP 87
38402 Saint-Martin d'Hères cedex, France

September 23, 2008

Abstract

Concentrated cell suspensions exhibit different mechanical behavior depending on the mechanical stress or deformation they undergo. They have a mixed rheological nature: cells behave elastically or viscoelastically, they can adhere to each other whereas the carrying fluid is usually Newtonian. We report here on a new elasto–visco–plastic model which is able to describe the mechanical properties of a concentrated cell suspension or aggregate. It is based on the idea that the rearrangement of adhesion bonds during the deformation of the aggregate is related to the existence of a yield stress in the macroscopic constitutive equation. We compare the predictions of this new model with five experimental tests: steady shear rate, oscillatory shearing tests, stress relaxation, elastic recovery after steady prescribed deformation, and uniaxial compression tests. All of the predictions of the model are shown to agree with these experiments.

1 Introduction

Cell aggregates or multicellular systems appear in several biological systems: embryo development [29, 28, 26, 39, 24], blood flow, hydra aggregates motion, dictyostelium slugs crawling [34, 33] and they are of considerable interest in tumor growth [1, 2, 15, 16, 42]. Their mechanical behavior is often assimilated to soft biological tissues, usually corresponding to viscoelastic materials or to non–Newtonian fluids [17].

On the other hand, it is known that the intrinsic properties of the base components - cells and collagen - as well as their concentration can influence the rheological properties of such aggregates [41]. The best example in this respect is provided by the early works of Chien on blood cell suspensions [8, 9]. He found that the mechanical properties of such suspensions are affected not only by the deformation of individual cells but also by the possible aggregation among cells. Macroscopically, cell aggregation gives rise to a yield stress, i.e. a characteristic tension that separates

the flow and solid regimes. Relationships between yield stress and individual cell properties, such as cell interfacial energy or their elastic moduli, has been provided relating the micro- and macro-properties by Snabre [37, 38]. Using this approach, Iordan *et al.* [20] were able to determine typical intrinsic properties for concentrated suspensions of Chinese Hamster Ovary cells (CHO).

Other works deal with different types of cell aggregates [13, 11, 12, 14, 42], and similar behaviors are observed. Their interpretation of the experimental data is usually given in terms of a macroscopic mechanism, i.e. the surface tension of the multicellular spheroid. Different values of the relevant parameter can be provided from studies dealing with heart, limb bud, liver, neural retina embryos. They show that cell aggregates can reorganize themselves like liquids with surface tension, as long as specific criteria are met for cell ordering [27, 5]. On the other hand, a yield stress might play a crucial role. In the typical compression experiment of Forgacs et al. [11], a fixed deformation is applied to the cell aggregate. The internal stress then relaxes until an asymptotic value is reached. This phenomenon could be explained using relaxation combined with a yield stress, as observed with other types of yield stress fluids of rheological interest [20, 32]. Therefore, models of viscoelastic behaviors coupled with a yield stress, although not yet much investigated, could be helpful in such cases [2, 35, 36]. Such models are called elasto-visco-plastic and have been applied in the past to various complex materials [19].

The purpose of this work is to compare the predictions of a visco-elasto-plastic model [2] with simple rheological experiments such as shear or compression tests. The model is illustrated in Section 2 and a linearized version is then discussed in Section 3. Steady shear is considered in Section 4.1 where the results are compared with relevant data [20], stress relaxation and oscillatory shear tests are discussed in Sections 4.2 and 4.3, elastic recovery after shear is illustrated in Section 4.4. In the last section, compression experiments similar to those performed in [11, 13, 14, 42] are re-considered in the framework of this new model.

2 Evolving Natural Configuration and Constitutive Model for Cell Aggregates

The present paper develops according to the arguments illustrated in [2], with one assumption that simplifies the algebraic aspects of the theory: as the time scale for cell mitosis and apoptosis is much larger then the typical time scale of mechanical experiments, here macroscopic growth is neglected; the focus is then on the plastic and elastic deformation and on the comparison with experiments known in the literature.

We will model cell suspensions and aggregates as continuum media. In fact, the cellular aggregates used in [11, 13, 14, 42] have a diameter ranging between 200 and 600 μm, which means a number of cells between ten and two hundred thousand. For the experiments by Iordan et al [20], the distance between the plates is 400 μm and the radius of the rheometer is 10 mm, so for a 40% suspension there are more than ten million cells. We also consider the ensemble of cells as a deformable porous material filled of physiological liquid. The volume ratio of the solid phase is denoted by ϕ. We assume that at equilibrium the inter–cellular fluid pressure is hydrostatic so that it plays no role in the dynamics. We therefore restrict to consider the dependence of the cellular volume fraction in the aggregate tension field.

A useful paradigm for elastoplastic deformations is the multiplicative decomposition of the deformation gradient $\mathbb{F}$ [22, 23]. This is a mapping from the tangent space related to the initial (reference) configuration $\mathcal{K}_0$ onto the tangent space related to the current configuration $\mathcal{K}$ and indicates how the body is deforming locally going from $\mathcal{K}_0$ to $\mathcal{K}$. A virtual intermediate configuration is then introduced, imagining that each point of the body is allowed to relieve its state of stress while relaxing the continuity requirement, i.e. the integrity of the body. It then relaxes to a stress-free configuration. The atlas of these pointwise configurations forms what we define natural configuration with respect to $\mathcal{K}$ and denote by $\mathcal{K}_n$.

The relaxed state $\mathcal{K}_n$ can differ from $\mathcal{K}_0$ because, during the deformation, cells in the configuration $\mathcal{K}_n$ can undergo internal re-organization, which implies re-arranging of the adhesion links

among the cells. We identify the deformation without cell re-organization with the tensor $\mathbb{F}_n$, describing how the body is deforming locally while going from the natural configuration $\mathcal{K}_n$ to $\mathcal{K}$. In this particular case, we will assume that for any given point the volume ratio in the natural configuration $\mathcal{K}_n$ and in the original reference configuration $\mathcal{K}_0$ are the same.

According to the two-step process outlined above, the deformation gradient is then split as

$$\mathbb{F} = \mathbb{F}_n \mathbb{F}_p. \tag{2.1}$$

In the following we will also use the following tensors

$$\mathbb{B}_n = \mathbb{F}_n \mathbb{F}_n^T\,, \qquad \mathbb{L} = \dot{\mathbb{F}}\mathbb{F}^{-1}\,, \qquad \mathbb{L}_p = \dot{\mathbb{F}}_p \mathbb{F}_p^{-1}\,, \quad \text{and} \qquad \mathbb{D}_p = \frac{1}{2}(\mathbb{L}_p + \mathbb{L}_p^T)\,. \tag{2.2}$$

where $\mathbb{B}_n$ is the left Cauchy-Green tensor related to the recoverable part of the deformation, while giving $\mathbb{L}_p$, or $\mathbb{D}_p$ will mean giving through the evolution of $\mathbb{F}_p$ information on the evolution of the natural configuration due to the internal re-organization of the cell and therefore on the irreversible part of the deformation.

Our aim is to include elasto-visco-plastic effects in the mechanics of cell aggregates detailing the constitutive equation for the stress tensor. The starting point of the theory is the following experimental evidence, that holds when a cell aggregate undergoes compression

1. for a moderate amount of stress, the cell aggregate deforms elastically;
2. above a yield value the cell aggregate undergoes internal re-organization which is modelled at a macroscopic level as a visco-plastic deformation.

The work needed to break a single cell-to-cell bond is measurable; the threshold of the onset of cell re-organization is proportional to the number of adhesion bonds or, in terms of surface density, it is proportional to the area of the cell membranes in contact times the bond energy [4], so that it depends on the number of cells per unit volume. Figure 1 is a photograph of a CHO cell suspension (Chinese Hamster Ovary, epithelial cell line, 52% concentration in culture medium). It illustrates the typical configuration of a cell aggregate: cells are packed, they touch each other and deform elastically, but they may shear and re-organize when a large enough stress is applied. We denote by $\tau(\phi)$ the minimum tension that induces the above shearing behavior and we call it the yield stress. In the following we will compare it with a frame invariant measure of the stress ($\phi\mathbb{T}$) of the cellular constituent, where $\mathbb{T}$ is the Cauchy stress tensor. It is worth to remark that the volume ratio is a macroscopic measure originated from an average and a small volume ratio can correspond to dispersed single cells as well as clusterized ensembles. In the former case, the yield stress is expected to be very low or null. In the second case, according to the theory of the dynamics of colloidal particles and flocculated suspensions, the yield stress should increase with the second or the third power of the volume ratio [7, 38, 8]. Iordan et al. [20] measured $\tau(\phi)$ to be proportional to $\phi^{8.4}$. They also find the dependence of the shear elastic modulus to vary like $\phi^{11.6}$, not very far from other recent results for weakly aggregated suspensions [32]. We expect that for cell aggregates like those used in [11, 13, 14, 42] the same mechanism holds, but of course the yield stress is much higher both because adhesion bonds have the necessary time to strengthen and because concentrations are higher in these works, giving rise to larger contact areas between cells.

On this basis, the following elastic-type constitutive equation can be suggested in the elastic regime

$$\mathbb{T} = \hat{\mathbb{T}}(\mathbb{B}_n)\,, \qquad \text{if} \quad f(\phi\mathbb{T}) \leq \tau(\phi)\,, \tag{2.3}$$

where f is a suitable measure of the stress. Basov and Shelukhin [3] suggest to use

$$\mathbf{t}(\mathbf{n}) = \phi[\mathbb{T}\mathbf{n} - (\mathbf{n}\cdot\mathbb{T}\mathbf{n})\mathbf{n}]\,, \tag{2.4}$$

that represents the tangential stress vector relative to the surface identified by the normal $\mathbf{n}$. In particular, we will use

$$f(\phi\mathbb{T}) = \max_{|\mathbf{n}|=1} |\mathbf{t}(\mathbf{n})|\,, \tag{2.5}$$

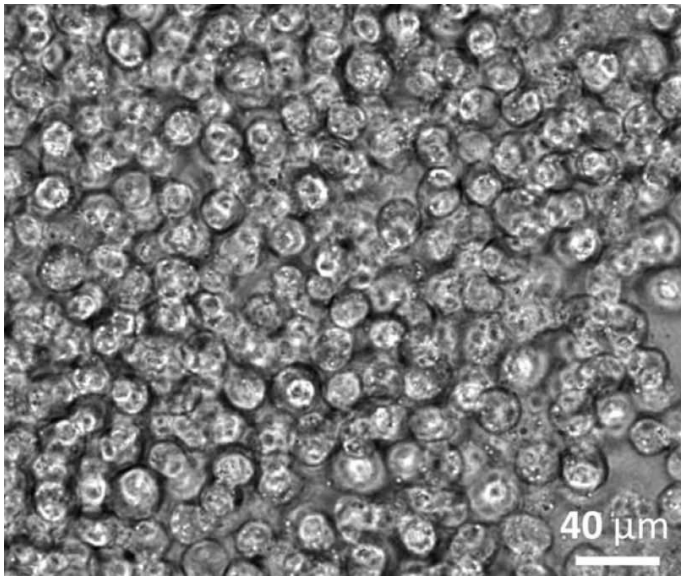

Figure 1: Photograph of a CHO cell suspension (epithelial cell type) at concentration $\phi = 0.52$.

representing the maximum shear stress magnitude occurring in the plane identified by the eigenvector corresponding to the maximum of $|\mathbf{t}(\mathbf{n})|$. It can be proved (see, for instance, [25]) that f is given by half of the difference between the maximum and the minimum eigenvalue of $\phi\mathbb{T}$. Also observe that $f(\mathbb{T}) = f(\mathbb{T}')$ where $\mathbb{T}' = \mathbb{T} - \frac{1}{3}(\mathrm{tr}\mathbb{T})\mathbb{I}$.

Now we assume that when the tension overcomes the yield stress in terms of the stipulated measure (2.11), the energy is no longer elastically stored. The extra energy is spent in cell unbinding at the microscopic scale, i.e. material rearrangement at the macroscopic scale. Cells flow in mutual direction, dissipating energy, and determining an evolution of the natural configuration. Such a pictorial description is put into formal terms by the following constitutive equation

$$\left[1 - \left(\frac{\tau(\phi)}{f(\phi\mathbb{T}')}\right)^{\alpha}\right](\phi\mathbb{T}') = 2\eta(\phi)\mathbb{F}_n\mathbb{D}_p\mathbb{F}_n^{-1}\,, \qquad \text{if} \quad f(\phi\mathbb{T}') > \tau(\phi)\,, \tag{2.6}$$

where $\mathbb{T}'$ operates on the current configuration and, for the sake of compatibility, $\mathbb{D}_p$ is pulled back using $\mathbb{F}_n$. As we shall see in Section 4, the exponent $\alpha \in [0, 1]$ determines the viscous behavior at high shear rates. It may be considered as an extra adjustable parameter necessary for obtaining better predictions like it is done in other constitutive equations for viscoelasticity. Here this is equivalent to having a new relaxation time which depends on α. This idea is already present in previous models (e.g., White-Metzner [6]). The idea is useful for predicting a shear-thinning behavior, which is not always the case (Oldroyd-B). This is precisely what we obtain here when α is varied: the shear thinning behavior (at large or moderate shear rates) is obtained and depends on α. Therefore α is similar to the index obtained for power law fluids, an index known to be related to the morphology of sub-structures formed by basic units (polymers, particules, fibers, cells, etc.) under flow. Unfortunately, we do not have any other data using different cell types like red blood cells with controlled mechanical properties. This is of course an interesting idea which deserves further work.

We can merge the above equation to the condition that there is no evolution of the natural configuration when and where the shear stress is smaller than the yield stress by writing

$$\mathbb{F}_n\mathbb{D}_p\mathbb{F}_n^{-1} = \frac{1}{2\tilde{\eta}}\left[1 - \frac{1}{\tilde{f}(\mathbb{T}')}\right]_+ \mathbb{T}'\,, \tag{2.7}$$

where $[\cdot]_+$ stands for the positive part of the argument, $\tilde{\eta} = \eta(\phi)/\phi$, and $\tilde{f}(\mathbb{T}') = [f(\phi\mathbb{T}')/\tau(\phi)]^{\alpha}$.

Rewriting the right hand side of Equation (2.7) in terms of $\mathbb{F}_p$ using the relation (2.2), it should clearly be understood that it is an evolution equation for the relaxed configuration. The switching of the positive part governed by the yield stress τ distinguishes between the elastic reversible behavior and the viscous irreversible behavior of cell aggregates.

In the following, we we assume that the elastic response of the cellular phase obeys a neo-Hookean law,

$$\mathbb{T} = \mu \mathbb{B}_n. \tag{2.8}$$

A neo-Hookean material is incompressible in bulk and therefore a scalar unknown field (the pressure) is needed the accomodate the constraint $\det \mathbb{B}_n = 1$ should appear in (2.8) in a one–component framework. However, a suspension or a cell aggregate are actually a mixture of incompressible components (cells and liquid) that can have different volumetric ratios the constrain being the saturation of the mixture. This constrain calls for an unknown scalar to be determined, the pressure of the mixture, (see Section 4.5).

In this case, $\mathbb{F}_p$ evolves according to

$$\dot{\mathbb{F}}_p = \frac{\mu}{\tilde{\eta}} \left[1 - \frac{1}{\mu \tilde{f} \left(\mathbb{B}_n - \frac{1}{3}(\mathrm{tr}\mathbb{B}_n)\mathbb{I} \right)} \right]_+ \mathbb{F}_n^{-1} \left(\mathbb{B}_n - \frac{1}{3}(\mathrm{tr}\mathbb{B}_n)\mathbb{I} \right) \mathbb{F}\,. \tag{2.9}$$

Eq. (2.9) can be phenomenologically explained in the following way: if the body undergoes a deformation corresponding to a stress below the yield stress, then the square parenthesis vanishes and $\mathbb{F}_p$ does not change, i.e., the natural configuration does not evolve and all the energy is stored elastically. If the measure of tension f takes a value larger than the yield stress, then the reference configuration changes to release the stress in excess, until the yield condition defined by f is reached again. The ratio $\tilde{\eta}/\mu$ gives an indication of the characteristic time needed to relax the internal stress through the re-organization of cells and to return the yield condition.

In order to merge Eq.(2.7) and Eq.(2.8) we derive

$$\mathbb{T}' = \mu \left(\mathbb{B}_n - \frac{1}{3}\mathrm{tr}\mathbb{B}_n\mathbb{I} \right)\,, \tag{2.10}$$

with respect to time. As shown in the Appendix, in a finite strain context one admissible time derivative is

$$\dot{\mathbb{B}}_n = \mathbb{L}\mathbb{B}_n + \mathbb{B}_n\mathbb{L}^T - 2\mathbb{F}_n\mathbb{D}_p\mathbb{F}_n^T\,, \tag{2.11}$$

and threfore

$$\dot{\mathbb{T}}' = \mu \left(\mathbb{L}\mathbb{B}_n + \mathbb{B}_n\mathbb{L}^T - 2\mathbb{F}_n\mathbb{D}_p\mathbb{F}_n^T - \frac{1}{3}\mathrm{tr}(\mathbb{L}\mathbb{B}_n + \mathbb{B}_n\mathbb{L}^T - 2\mathbb{F}_n\mathbb{D}_p\mathbb{F}_n^T)\mathbb{I} \right)\,. \tag{2.12}$$

Using (2.7) to eliminate $\mathbb{D}_p$, one then has

$$\dot{\mathbb{T}}' + \frac{\mu}{\tilde{\eta}} \left[1 - \frac{1}{\tilde{f}(\mathbb{T}')} \right]_+ \left(\mathbb{T}'\mathbb{B}_n - \frac{1}{3}\mathrm{tr}(\mathbb{T}'\mathbb{B}_n)\mathbb{I} \right) = \mu \left[\mathbb{L}\mathbb{B}_n + \mathbb{B}_n\mathbb{L}^T - \frac{1}{3}\mathrm{tr}(\mathbb{L}\mathbb{B}_n + \mathbb{B}_n\mathbb{L}^T)\mathbb{I} \right]\,, \tag{2.13}$$

which can be written in terms of upper convected derivative

$$\frac{\mathcal{D}\mathbb{M}}{\mathcal{D}t} = \dot{\mathbb{M}} - \mathbb{L}\mathbb{M} - \mathbb{M}\mathbb{L}^T\,, \tag{2.14}$$

as

$$\frac{\mathcal{D}\mathbb{T}'}{\mathcal{D}t} + \frac{1}{\lambda} \left[1 - \frac{1}{\tilde{f}(\mathbb{T}')} \right]_+ \left(\mathbb{T}'\mathbb{B}_n - \frac{1}{3}\mathrm{tr}(\mathbb{T}'\mathbb{B}_n)\mathbb{I} \right) = \frac{2}{3}\mu \left[\mathrm{tr}(\mathbb{B}_n)\mathbb{D} - \mathrm{tr}(\mathbb{B}_n\mathbb{D})\mathbb{I} \right]\,, \tag{2.15}$$

where $\lambda = \frac{\tilde{\eta}}{\mu}$ will be called here the *plastic rearrangement time*. Notice that (2.13) and (2.15) do not depend on $\mathbb{F}_p$, but only on quantities related to the deformation of the body and to the recoverable part of the deformation.

3 Small Deformations from the Evolving Natural Configuration

In what follows we assume that the deformation from the natural configuration is small. This assumption applies depending on the value of the yield stress: it has to be small enough so that the condition $|\mathbb{B}_n \cdot \mathbb{I} - 3| \ll 1$ is always satisfied during the motion. The experiments by Iordan et al. [20] give an indication of the order of magnitude of the yield stress. In this regime of small strain linear elasticity applies. Notice that there is no smallness assumption on $\mathbb{F}$, that can actually be large. The introduction of this approximation yields a simplified constitutive equation that, however, will no longer be objective and will only be valid when the deformation from the evolving natural configuration is small.

In the limit of small elastic deformations

$$\mathbb{L}\mathbb{B}_n + \mathbb{B}_n\mathbb{L}^T \approx 2\mathbb{D}\,, \qquad \text{and} \qquad \mathbb{T}'\mathbb{B}_n \approx \mathbb{T}'\,, \tag{3.1}$$

and therefore (2.13) simplifies to

$$\dot{\mathbb{T}}' + \frac{1}{\lambda}\left[1 - \frac{1}{\tilde{f}(\mathbb{T}')}\right]_+ \mathbb{T}' = 2\mu\left(\mathbb{D} - \frac{1}{3}(\mathrm{tr}\mathbb{D})\,\mathbb{I}\right)\,. \tag{3.2}$$

We observe that in equation (3.2), the term containing the yield stress plays the role of a stress relaxation term but it switches on just when the stress is above the yield value. Otherwise, for $\tilde{f}(\mathbb{T}') < 1$, equation (3.2) can be integrated in time to give back the elastic relation (2.10).

Similarly to classical viscoelasticity [18, 21], here the plastic rearrangement time λ identifies the characteristic time needed to relax the stress to the yield value (not the null one, as in Maxwell fluids).

Following the same argument proposed in [30, 31] one can state that in transient phenomena for times much larger than the *plastic rearrangement time* the natural configuration evolves relaxing the stress and dissipation stops when the state of stress of the material reaches the surface identified by the yield condition.

4 Applications

We now want to analyze the behavior of the constitutive model introduced in the previous sections under different shear and compression tests.

For pure shear tests (3.2) rewrites

$$\dot{T} + \frac{1}{\lambda}\left[1 - \left(\frac{\hat{\tau}}{|T|}\right)^{\alpha}\right]_+ T = \mu\dot{\gamma}\,, \tag{4.1}$$

where $\dot{\gamma}$ is the shear rate, $f(\mathbb{T}) = |T_{xy}| = |T|$ and $\hat{\tau} = \tau(\phi)/\phi$. The case $\alpha = 1$ corresponds to a Bingham fluid while the limit case $\alpha = 0$ corresponds to an elastic fluid. In the following, sometimes the particular case $\alpha = 1$ will be considered in more detail, because it allows to write analytical solutions in an easy way and to easily understand the main feature of the constitutive model.

4.1 Steady shear

According to the model illustrated in the previous section, when a cell aggregate undergoes a standard shear test with smooth loading, initially the body deforms elastically and the stress grows until the yield value $\hat{\tau}$ is reached. In this initial regime the cell bonds are simply stretched, no internal re-organization occurs, the natural configuration does not evolve, and the body would be able to return to the initial stress-free configuration. When locally the stress overcomes the

yield value, some adhesion bonds break, new ones form and the natural configuration evolves. The body is then not able to return to the original configuration any longer.

As an example, consider the case of shear increasing linearly in time, i.e., $\gamma = \dot{\gamma}_0 t$ and $\alpha = 1$. Integration in time of (4.1) gives

$$T(t) = \begin{cases} \mu\dot{\gamma}_0 t\,, & \text{for} \quad t \le t_\tau = \frac{\hat{\tau}}{\mu\dot{\gamma}_0}\,; \\ \\ \hat{\tau} + \mu\dot{\gamma}_0\lambda\left[1 - e^{(-t+t_\tau)/\lambda}\right]\,, & \text{for} \quad t > t_\tau\,. \end{cases} \tag{4.2}$$

If $t \to \infty$ then $T(t) \to \hat{\tau} + \tilde{\eta}\dot{\gamma}_0$. This means that plotting the apparent viscosity $\eta(\dot{\gamma}_0) = T/\dot{\gamma}_0$ as a function of the shear rate $\dot{\gamma}_0$, the plot should depend on $\dot{\gamma}_0^{-1}$ for small $\dot{\gamma}_0$. This is the case of experiments shown in [20].

In general, for $0 \le \alpha \le 1$, the relation between $\dot{\gamma}_0$ and the apparent viscosity $\eta(\dot{\gamma}_0)$ is given by

$$\dot{\gamma}_0 = \frac{\hat{\tau}}{\eta(\dot{\gamma}_0)}\left(1 - \frac{\tilde{\eta}}{\eta(\dot{\gamma}_0)}\right)^{-1/\alpha}\,. \tag{4.3}$$

If $\eta \to \infty$ then $\dot{\gamma}_0$ goes to zero as $\hat{\tau}/\eta(\dot{\gamma}_0)$ that implies that for small $\dot{\gamma}_0$, the apparent viscosity $\eta(\dot{\gamma}_0)$ behaves like $\dot{\gamma}_0^{-1}$. On the other hand, if $\eta \to \tilde{\eta}$ then $\dot{\gamma}_0$ goes to infinity, that means that at high shear rates, the apparent viscosity $\eta(\dot{\gamma}_0) = T/\dot{\gamma}_0$ goes towards its limiting value $\tilde{\eta}$. This limit is concentration dependent and has been obtained experimentally [10, 20]. A plot of the viscosity dependence against shear rate is presented in Fig.2a. One can note the limiting behaviors at small shear rates (slope -1 on this log–log figure). At high $\dot{\gamma}_0$, the viscosity reaches its limit $\tilde{\eta}$.

In order to observe the behavior close to the limit $\tilde{\eta}$, a plot of the reduced viscosity $\frac{\eta(\dot{\gamma}_0)-\tilde{\eta}}{\tilde{\eta}}$ is shown in Fig.2b and the limiting behavior for high shear rates can be explained. Noting that (4.3) can be partly inverted, it is obtained that

$$\frac{\eta(\dot{\gamma}_0) - \tilde{\eta}}{\tilde{\eta}} = \frac{\eta(\dot{\gamma}_0)}{\tilde{\eta}}\left(\frac{\eta(\dot{\gamma}_0)\dot{\gamma}_0}{\hat{\tau}}\right)^{-\alpha}.$$

Therefore, as $\eta(\dot{\gamma}_0)$ approaches $\tilde{\eta}$ in the high shear rate domain,

$$\frac{\eta(\dot{\gamma}_0) - \tilde{\eta}}{\tilde{\eta}} \sim \left(\frac{\tilde{\eta}\dot{\gamma}_0}{\hat{\tau}}\right)^{-\alpha}\,.$$

This means that in a log-log plot a slope of $-\alpha$ should be obtained as the apparent viscosity approaches $\tilde{\eta}$ for large shear rates $\dot{\gamma}_0$, as shown in Fig.2b. So, a crucial role in the constitutive model is played by the term $\tilde{f}(\mathbb{T}')$ that compares the scalar invariant measure of the stress with the yield stress $\hat{\tau}$ and determines the Bingham-like behavior at low shear rates, where the curves collapse. The role of the coefficient α becomes evident at high shear rates where it has an effect on the values of the viscosity. In fact, α is the slope of $\frac{\eta(\dot{\gamma}_0)-\tilde{\eta}}{\tilde{\eta}}$ vs. $\dot{\gamma}$ in log–scale. So, its role becomes important in catching the high flow rate behavior of the suspension of cells, when, probably, the suspension of cells may spatially re-arrange giving rise to aligned structures.

In order to validate the model with a true biological aggregate, parameter adjustements are made using the data of Iordan et al. [20] in Fig.3b. The only adjustable parameters are found to be $\frac{\hat{\tau}}{\tilde{\eta}}$ and α, by simple scaling arguments. In our case, we fixed $\tilde{\eta} = 0.0013\,Pa.s$ (the culture medium viscosity) and let $\hat{\tau}$ and α vary. A first attempt is made on the 42% concentration and values of the fitting parameters give $\hat{\tau} = 0.05Pa$ and $\alpha = 0.01$. This is shown in Fig.3b.

Again, we carry on the same type of analysis and this gives rise to the following features in Fig.3a. We obtained that, in most cases, $0.001 \le \alpha \le 0.01$, using the same $\tilde{\eta} = 0.0013\,Pa \cdot s$. The values of the yield stress are found to be close to the ones obtained previously [20] and show a typical dependence of the type $\hat{\tau} \sim 962.2\,\phi^{11}$, at large concentrations $0.4 \le \phi \le 0.6$. The small values found for α indicate that the system has some elastic properties, which will be discussed in Section 4.2.

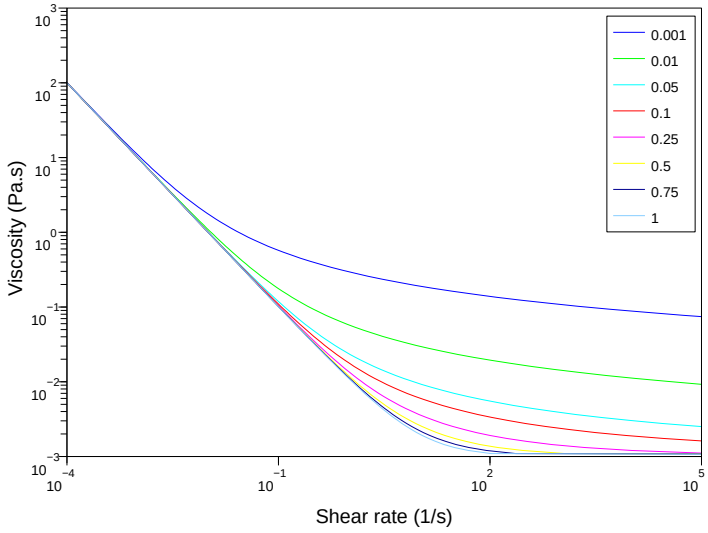

(a)

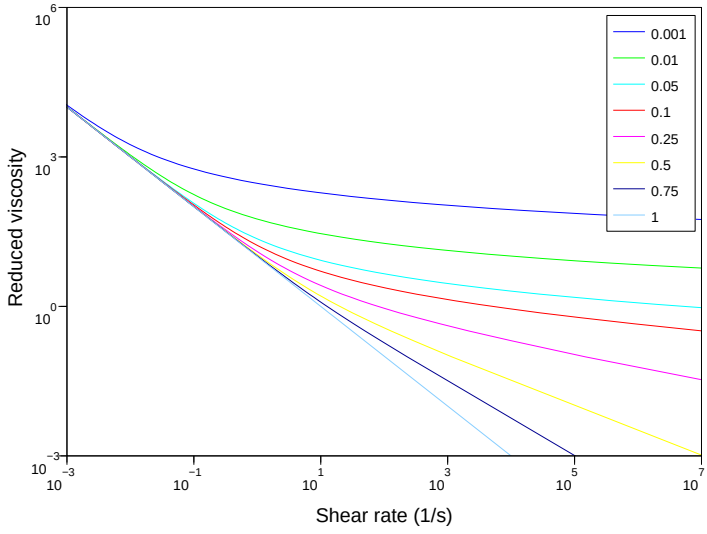

(b)

Figure 2: Apparent viscosity $\eta(\dot{\gamma}_0) = T/\dot{\gamma}_0$ and reduced viscosity $\frac{\eta(\dot{\gamma}_0)-\tilde{\eta}}{\tilde{\eta}}$ for different values of the parameter α.

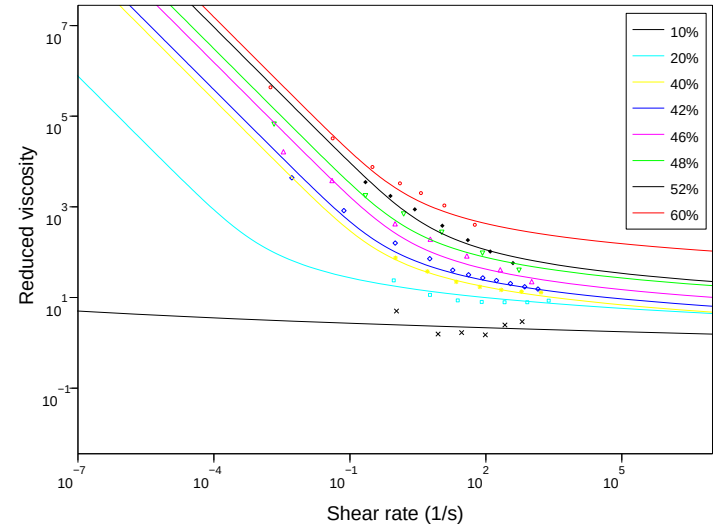

(a)

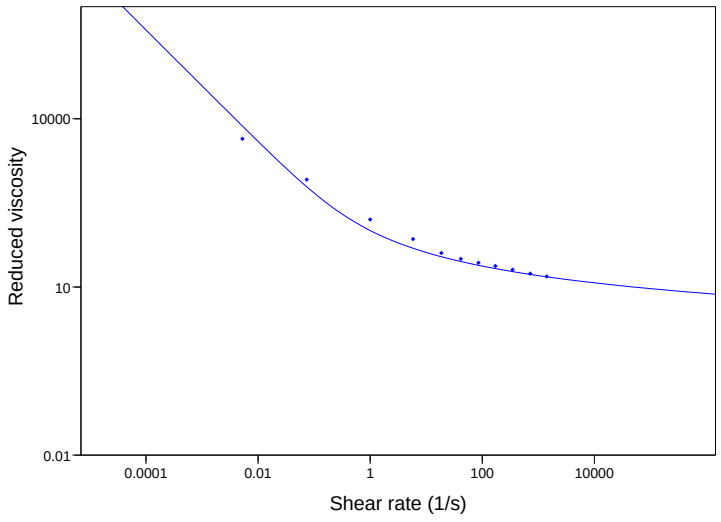

(b)

Figure 3: Comparison of the model vs. the experiments by Iordan et al. [20]. (a) Viscosity vs. shear rate at different volume ratios. (b) focuses on the case $\phi = 0.42$. Fitting parameters are $\hat{\tau} = 0.05\,Pa, \tilde{\eta} = 0.0013\,Pa \cdot s, \alpha = 0.01$.

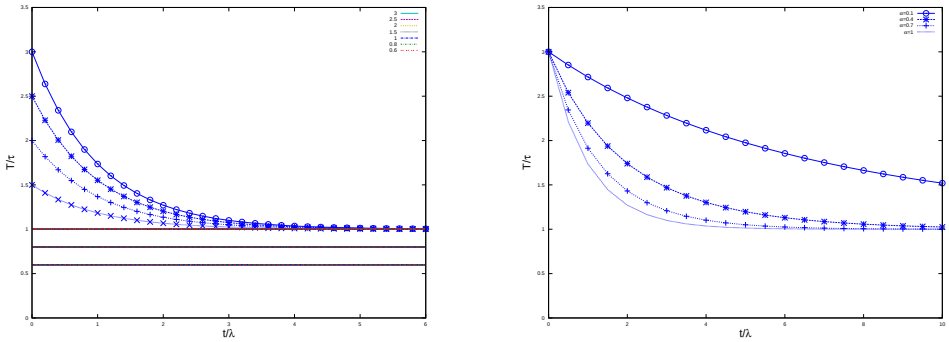

(a) (b)

Figure 4: Stress relaxation response (Time is normalized with respect to λ.) (a) $T/\hat{\tau}$ for different values of $\mu\gamma_0/\hat{\tau}$ and $\alpha = 1$. For $\gamma_0 \leq \hat{\tau}/\mu$ the response is elastic. (b) Evolution of $T/\hat{\tau}$ for $\mu\gamma_0/\hat{\tau} = 3$ and for increasing values of α (from upper to lower curves).

Finally, we observe that if $\alpha = 1/2$ then the steady response would satisfy

$$\sqrt{T} = \sqrt{\hat{\tau}} + \frac{\eta}{\sqrt{T}}\dot{\gamma}_0\,,$$

that can be solved to give

$$\sqrt{T} = \sqrt{\frac{\hat{\tau}}{4}} + \sqrt{\frac{\hat{\tau}}{4} + \eta\dot{\gamma}_0}\,,$$

that is close to the classical Casson's relation $\sqrt{T} = \sqrt{\hat{\tau}} + \sqrt{\eta\dot{\gamma}_0}$.

We conclude that, despite its simplicity, the model agrees quite well with the data obtained in [20].

4.2 Stress relaxation

A standard relaxation test is obtained applying a sudden constant deformation γ_0. If $\gamma_0 \leq \hat{\tau}/\mu$, then the stress in the body is $T = \mu\gamma_0 (< \hat{\tau})$ at any time corresponding to the straight line in Fig.4a, an elastic response. If, on the other hand, $\gamma_0 > \hat{\tau}/\mu$ the solution of Eq.(4.1) is

$$T(t) = \hat{\tau}\left\{1 + \left[\left(\frac{\mu\gamma_0}{\hat{\tau}}\right)^{\alpha} - 1\right] e^{-\alpha t/\lambda}\right\}^{1/\alpha}\,, \tag{4.4}$$

and is plotted in Fig.4a for increasing values of γ_0 and in Fig.4b for different α's. In particular, for $\alpha = 1$

$$T(t) = \hat{\tau} + (\mu\gamma_0 - \hat{\tau})e^{-t/\lambda}\,. \tag{4.5}$$

Hence for small strains the body behaves elastically, while for large strains part of the stress relaxes to the yield value $\hat{\tau}$, regardless of the magnitude of the applied strain. Notice that the decrease toward the asymptotic state is faster for larger exponents.

4.3 Oscillatory shear

Oscillatory shear experiments are a common technique to characterize viscoelastic materials without much deforming the samples. Experiments of this type have been carried out using red blood cell suspensions [40] or recently with CHO cell suspensions [20].

The usual protocol way to do this is to apply a sinusoidal deformation $\gamma = \gamma_0 \sin(\omega t)$ and plot the stress response $T = T_0 \sin(\omega t + \psi)$. Here ω is the angular frequency, ψ the phase

angle, γ_0 the applied deformation and T_0 the stress amplitude. Typically, small deformations are used in order to remain in the linear regime. Therefore, one can define the elastic and viscous moduli (G', G'') which correspond respectively to the in–phase part of the stress (G') and out of phase part (G''). Typical moduli responses [20] vs. frequency in the case of concentrated cell suspensions usually show a plateau for the G' modulus whereas G'' usually increases slowly with frequency. Similarly, using red blood cell suspensions, Thurston [40] observed the appearance of a high elasticity (increasing values of G' vs. frequency) for higher concentrations of cells (typically 70%).

Researchers have used this method also for large deformations [19] thus obtaining a variety of results that are understood as the signature of complex fluids. Note that the stress response now includes other frequency modes such as $\omega, 3\omega...$ In such a case, the values of moduli G' and G'' are plotted against the amplitude of the applied deformation γ_0, and usually show a decreasing behavior as in polymeric systems. Recently [19, 35], it has been found that other behaviors like strain hardening possibly followed by a decrease in G' or G'' could be observed with complex materials and this could be an interesting way to classify such a complexity.

Considering first small deformations and using (4.1) with the above applied sinusoidal deformation, we obtain an elastic behavior, when stresses are smaller than the yield stress $\hat{\tau}$:

$$\dot{T} = \mu\dot{\gamma} = \mu\omega\, cos(\omega t) \tag{4.6}$$

Therefore, the complex moduli $G^* = G' + iG''$ is simply $G^* = \mu$. Note that normal stresses are neglected here, but could be included leading to slight changes in the moduli evolution [35]. This result is therefore not good enough to describe the behavior of aggregates as observed in our earlier work [20], although the behavior for G' is characteristic of such aggregates.

We next consider the resolution of (4.1) using a periodic sine wave for a large amplitude deformation. Results are shown in Fig.5a. The shear stress follows the oscillatory motion imposed by the deformation as long as it is below the yield stress $\hat{\tau}$ but as it becomes higher, it follows a more complex time dependence. G' and G'' can be deduced from the stress amplitude by Fourier transform providing the first modes $\sin(\omega t)$ and $\cos(\omega t)$. They are plotted in Fig.5b. G' is a constant equal to μ then decreases with deformation, at a critical deformation $\gamma_c \sim 0.01$. This critical value corresponds to the fact that the shear stress reaches the critical value $\hat{\tau} = \mu\gamma_c = 1Pa$ in this case. On the other hand, G'' increases from 0 to reach a maximum then decreases again with deformation or shows a plateau. This is usually the behavior called "weak strain overshoot" as obtained previously for Xanthan gum solutions [19, 35, 36].

The value of γ_c is found to be close to 1% (deformation of 0.01), even when the frequency is changed. As shown in Fig.5b, as ω increases, G' decreases in a less pronounced manner, and the loss modulus G'' decreases more slowly, except for the last case corresponding to an angular frequency $\omega = 500\, rad/s$, when it always increases.

4.4 Elastic recovery

To compare the predictions of the mathematical model illustrated above and the experimental results obtained by Foty et al. [12], we now consider a modification of the stress relaxation experiment consisting in releasing the imposed stress after some time from the beginning of the experiment. As already stated, if the imposed deformation is small as compared to the yield condition, then the body will go back to the original configuration. Otherwise, it induces an internal re-organization of the cells and the body will not recover its initial configuration, because in the meantime the natural configuration has changed. In fact, denoting by T_2 the value of stress before the sudden stress release (that is much faster than the cell re-organization time λ) the yield stress is reached for

$$\gamma = \gamma_2 - \frac{T_2 - \hat{\tau}}{\mu}\,, \tag{4.7}$$

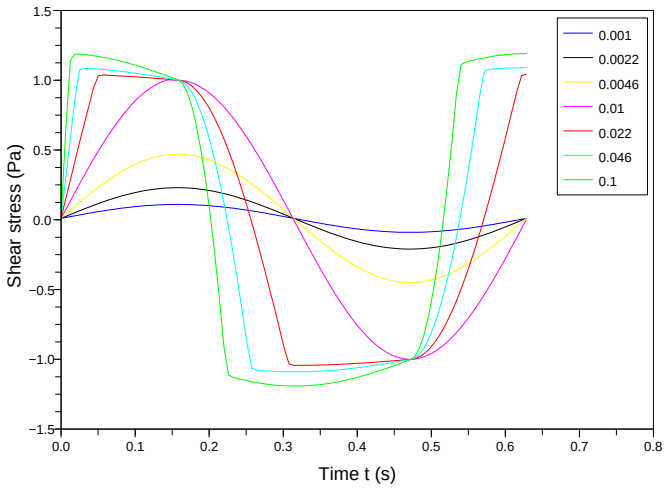

(a)

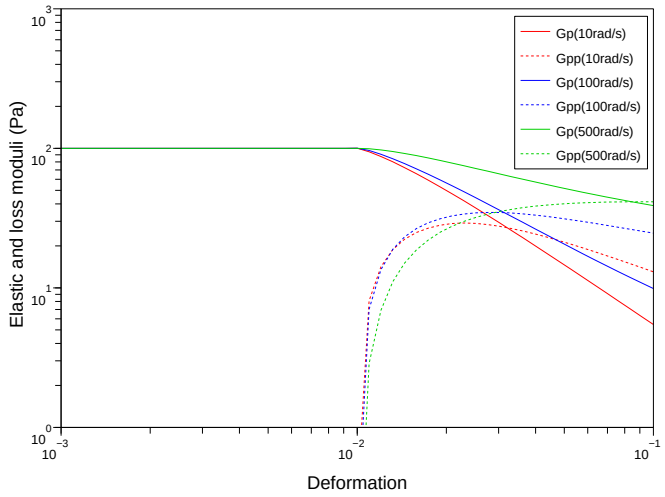

(b)

Figure 5: Stress response when applying a sinusoidal deformation. Parameters: $\eta = 0.17Pa \cdot s$, $\mu = 100Pa$, $\hat{\tau} = 1Pa$, $\alpha = 0.5$, $\lambda = 0.001\,s$. (a) Different stress responses for different $\gamma_0 = 0.001, 0.0022, 0.0046, 0.01, 0.022, 0.046, 0.1$. The response becomes nonlinear above 1% deformation. (b) Moduli G' (Gp) and G'' (Gpp) vs. deformation at different angular frequencies $\omega = 10 - 100 - 500\,rad/s$.

independently of α. After that, the body will relax the stress, reaching the stress-free configuration when

$$\gamma_{\text{fin}} = \gamma_2 - \frac{T_2}{\mu}\,. \tag{4.8}$$

To be more specific, in the stress relaxation experiment described by Eq.(4.4), at time t_{compr} the compressing plate is removed so that the specimen is stress-free and

$$\gamma_{\text{fin}} = \gamma_0 - \frac{\hat{\tau}}{\mu}\left\{1 + \left[\left(\frac{\mu\gamma_0}{\hat{\tau}}\right)^{\alpha} - 1\right] e^{-\alpha t_{compr}/\lambda}\right\}^{1/\alpha}\,. \tag{4.9}$$

In particular, if $t_{compr} \ll \lambda$, the exponential and the power in (4.9) can be approximated to give

$$\gamma_{\text{fin}} \approx \gamma_0 \left[1 - \left(\frac{\hat{\tau}}{\mu\gamma_0}\right)^{\alpha}\right] \frac{t_{compr}}{\lambda}\,. \tag{4.10}$$

This means that if the compression is kept for such a small time that the body does not have enough time to re-organize, then the body will recover almost everything and return close to the original configuration mainly showing an elastic-like behavior. If, on the other hand, $t_{compr} \gg \lambda$, then

$$\gamma_{\text{fin}} = \gamma_0 - \frac{\hat{\tau}}{\mu}\,, \tag{4.11}$$

meaning that the body will still recover the amount $\hat{\tau}/\mu$ corresponding to the elastic component. In other words, it will not keep the value $\gamma = \gamma_0$ imposed, even if this is done for a very long time.

The above description is consistent with the observations in [12] (their figures 3 and 5) where they see that if the spheroid is compressed for few seconds then it will bounce back almost to the original configuration. If it is compressed for a longer time (few hours in their experiments) this does not occur though a minor shape recovery is observed. This can not be explained using the concept of surface tension, but is compatible with our model.

On the other hand, we have to point out that in this model the process is instantaneous, while it seems that in the experiment in [12] it takes some times for the spheroid to return to the natural configuration as in standard indentation tests. This might be due to the fact that here we completely neglected the fact that the spheroid is a porous material filled with the liquid in which the experiment is done. Such an effect can be included for instance taking into account that T is only one of the components of the stress and a further viscous component needs to be added to obtain the stress for the mixture as a whole T_m, i.e.,

$$T_m = T + \eta_\ell \dot{\gamma}\,. \tag{4.12}$$

In this case the process will take a characteristic time of the order of $\lambda/(1 + \frac{\tilde{\eta}}{\eta_\ell})$.

4.5 Uniaxial compression

In this section we study the response of a material satisfying (3.2) subjected to a uniaxial compression test in order to qualitatively compare our model with the experimental results described in [11, 12, 42].

We will assume that the deformation is homogeneous and is given by

$$x = \frac{X}{\sqrt{\psi(t)}}\,, \qquad y = \frac{Y}{\sqrt{\psi(t)}}\,, \qquad z = \psi(t)Z\,, \tag{4.13}$$

with $\mathbb{F}_p$ given by

$$\mathbb{F}_p = \operatorname{diag}\left\{\frac{1}{\sqrt{\Psi(t)}}, \frac{1}{\sqrt{\Psi(t)}}, \Psi(t)\right\}\,. \tag{4.14}$$

The difference between $\Psi(t)$ and 1 is a measure of aggregate re-organization. Hence $\mathbb{F}$ and $\mathbb{F}_n$ are respectively given by

$$\mathbb{F} = \mathrm{diag}\left\{\frac{1}{\sqrt{\psi(t)}}, \frac{1}{\sqrt{\psi(t)}}, \psi(t)\right\}, \tag{4.15}$$

and

$$\mathbb{F}_n = \mathrm{diag}\left\{\sqrt{\frac{\Psi(t)}{\psi(t)}}, \sqrt{\frac{\Psi(t)}{\psi(t)}}, \frac{\psi(t)}{\Psi(t)}\right\}. \tag{4.16}$$

Therefore, dropping t for sake of simplicity,

$$\mathbb{B}_n = \mathrm{diag}\left\{\frac{\Psi}{\psi}, \frac{\Psi}{\psi}, \frac{\psi^2}{\Psi^2}\right\}, \tag{4.17}$$

and

$$\mathbb{T} = \mu\,\mathrm{diag}\left\{-\Sigma + \frac{\Psi}{\psi}, -\Sigma + \frac{\Psi}{\psi}, -\Sigma + \frac{\psi^2}{\Psi^2}\right\} = \mathrm{diag}\{0, 0, P_{\mathrm{appl}}\}, \tag{4.18}$$

where Σ is the pressure of the mixture and P_{appl} is the time–dependent applied stress in the z-direction.

In conclusion,

$$\Sigma = \frac{\Psi}{\psi}, \quad \text{and} \qquad P_{\mathrm{appl}} = \mu\frac{\psi^3 - \Psi^3}{\psi\Psi^2}. \tag{4.19}$$

On the other hand,

$$\mathbb{D}_p = \dot{\mathbb{F}}_p\mathbb{F}_p^{-1} = \mathrm{diag}\left\{-\frac{1}{2}, -\frac{1}{2}, 1\right\}\frac{\dot{\Psi}}{\Psi}, \tag{4.20}$$

and therefore from (2.7)

$$\frac{\dot{\Psi}}{\Psi} = \frac{1}{3\tilde{\eta}}\left[1 - \frac{1}{\tilde{f}(\mathbb{T}')}\right]_+ P_{\mathrm{appl}} = \frac{1}{3\tilde{\eta}}\left[1 - \left(\frac{2\hat{\tau}}{|P_{\mathrm{appl}}|}\right)^{\alpha}\right]_+ P_{\mathrm{appl}}. \tag{4.21}$$

Substituting (4.19) in the equation above, one has the evolution equation for Ψ, i.e., for the natural configuration

$$\frac{\dot{\Psi}}{\Psi} = \frac{\mu}{3\tilde{\eta}}\left[1 - \left(\frac{2\hat{\tau}}{\mu}\,\frac{\psi\Psi^2}{|\psi^3 - \Psi^3|}\right)^{\alpha}\right]_+ \frac{\psi^3 - \Psi^3}{\psi\Psi^2}. \tag{4.22}$$

This result applies to a parallelepiped sample homogeneously deformed in uniaxial traction. In the following we compare its predictions with the stress-strain behavior of a loaded multicellular spheroid. The latter problem clearly involves a non–homogeneous deformation and a purely qualitative comparison can be carried out at most.

When a sufficiently large strain $\psi_0 < 1$ is imposed on the cell aggregate, the square parenthesis above is positive, i.e.,

$$\frac{1}{\psi_0} - \psi_0^2 > \frac{2\hat{\tau}}{\mu}, \tag{4.23}$$

Ψ will decrease from $\Psi = 1$ according to

$$\dot{\Psi} = -\frac{\mu}{3\tilde{\eta}}\left[1 - \left(\frac{2\hat{\tau}}{\mu}\,\frac{\psi_0\Psi^2}{\Psi^3 - \psi_0^3}\right)^{\alpha}\right]\frac{\Psi^3 - \psi_0^3}{\psi_0\Psi}. \tag{4.24}$$

A plot of $\Psi(t)$ is shown in Fig. 6.

If the compression applies for a long enough time, then Ψ will tend towards that value $\Psi_\infty > \psi_0$ corresponding to the vanishing of the square parenthesis in (4.24), i.e.,

$$\frac{\Psi_\infty^3 - \psi_0^3}{\psi_0\Psi_\infty^2} = \frac{2\hat{\tau}}{\mu}, \tag{4.25}$$

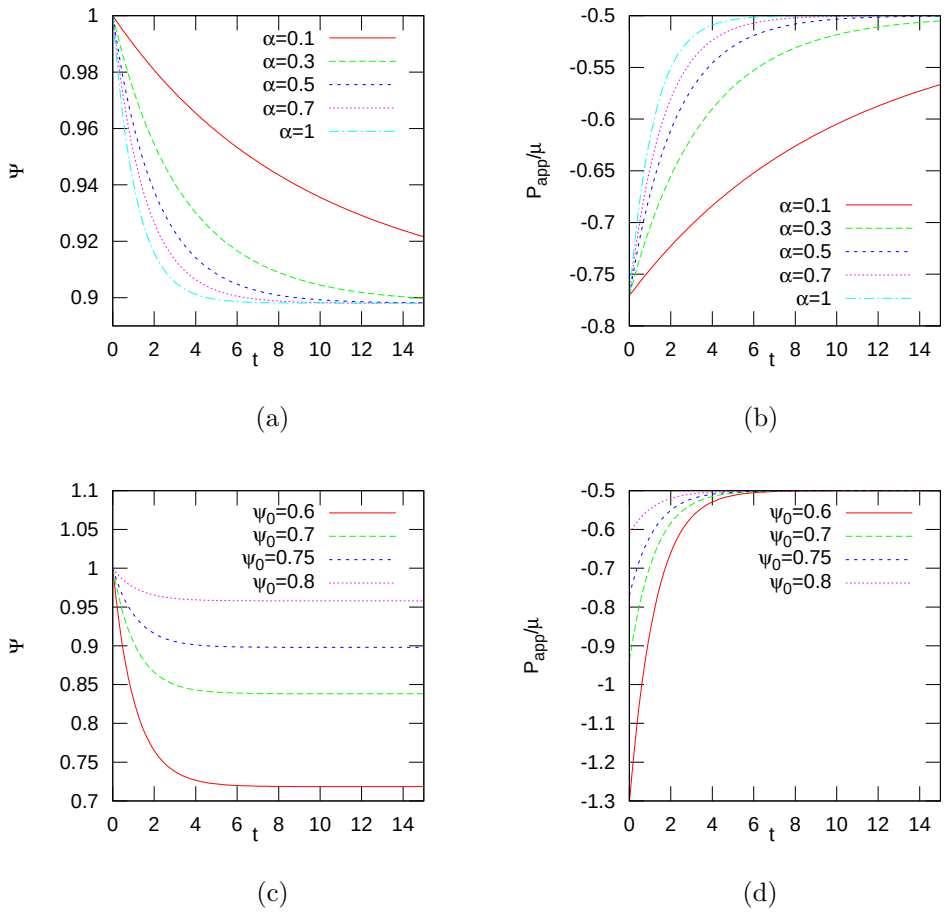

Figure 6: Uniaxial compression for $\hat{\tau}/\mu = 0.25$. Time is normalized with respect to $\tilde{\eta}/\mu$ and the applied stress is reported normalized with respect to μ. In (a,b) $\psi_0 = 0.75$ and $\alpha = 0.1, 0.3, 0.5, 0.7, 1$. In all cases the asymptotic value of Ψ is $\Psi_\infty = 0.8981$ and P_{appl}/μ tends to $2\hat{\tau}/\mu = -0.5$. In (c,d) α is fixed to 1 while ψ_0 changes. If $\psi_0 > 0.8351$ the compression is not strong enough to trigger cell re-organization and therefore $\Psi(t) = 1$ does not evolve and $P_{\rm appl}/\mu$ is constantly equal to $\psi_0^2 - 1/\psi_0 > -0.5$.

that is independent of α, as also evident from Figures 6a.

In particular, P_{appl} will tend to

$$P_{\text{appl},\infty} = \mu \frac{\psi_0^3 - \Psi_\infty^3}{\psi_0 \Psi_\infty^2} = -2\hat{\tau}\,, \tag{4.26}$$

(see Fig. 6b,d) that in addition of being independent of α is also independent of ψ_0 as in the experiments in [11].

In Fig. 6c,d instead the value of α is fixed to 1 and different compressions are applied. If $\psi_0 > 0.8351$ the compression is not strong enough to trigger cell re-organization and therefore $\Psi(t) = 1$ does not evolve and $|P_{\text{appl}}|$ is constantly below the yielding value that in this case is $2\hat{\tau} = 0.5$. For larger ψ_0 the natural configuration evolves and P_{appl} again tends to the constant value given in (4.26).

The behavior of the solution is then similar to the shear tests discussed in Section 4.4. Finally, if at time t_2 (when $\Psi = \Psi_2 > \Psi_\infty$), the compression is suddenly released, then ψ will readily adjust to the value $\psi = \Psi_2$.

Although this solution strictly applies to a parallelepiped sample, we qualitatively compare it with the stress relaxation tests performed by Forgacs et al. [11] for a spheroid. The main remark is that the measured stress decreases asymptotically to a non-null value that depends on the tissue.

They interpret this long time behavior as the effect of surface tension that can be obtained multiplying the measured stress by a coefficient that depends on the geometry of the barrel shape of the deformed aggregate. In Winters et al. [42] it is observed that doubling the deformation will give rise to the similar surface tension coefficient, while a constitutive model for a linear elastic solid whould give rise to a doubling of the stress.

In our view the same result can be interpreted using the constitutive model above and relating the asymptotic behavior to a measure of the yield stress. In fact, similarly to the experiments above, in the present virtual experiment (that does not present a free boundary) doubling the deformation will give rise to the same asymptotic value measuring the yield stress.

The relation between the two interpretations is given by $\hat{\tau} = H\sigma$ where σ is the surface tension and H is the mean curvature of the compressed spheroids. Though it is difficult to get the geometrical parameters from the paper, using the values in Forgacs et al. [11] it seems that the yield stress for the different tissues tested ranges between 1 to 100 Pa. Our results for a 60% concentration (the maximum one that we used) give a yield stress around $2Pa$, and higher concentrations will probably lead to data in the same range, especially since the yield stress is concentrated dependent like $\hat{\tau} \sim \phi^{11}$, as observed previously.

Furthermore, Foty and Steinberg [14] correlate the surface tension coefficient with the density of surface cadherin per cell. The same proportionality obviously holds for the yield stress $\hat{\tau}$ because this coefficient is clearly related to the number of adhesion bonds. In our opinion the relation between yield stress and surface tension also explains the observation by Winters et al [42] that cell invasiveness is related to the inverse of surface tension: the smaller the adhesion between cells, the smaller the yield stress, the more invasive the cell clone.

We finally mention that Forgacs et al. [11] point out the existence of two relaxation times in the cellular matter (one of the order of few seconds the other of the order of tens of seconds), that in our approach would be related to two re-organization mechanisms or to the detachment of different types of adhesion proteins. Of course, our model can be generalized to include more relaxation times.

5 Conclusions and Developments

In this paper we have derived a constitutive model that is able to describe the twin characteristics of cell aggregates: solid-like when and where the stresses are not large enough and liquid-like when and where the stress overcomes a sustainable threshold inducing internal cell re-organization. Though the constitutive model is kept as simple as possible, we have shown how it can reproduce the outcome of both shear tests performed by [20] and compression tests performed by [11, 13,

12, 14, 42]. The model also enabled us to predict the nonlinear dynamic shear behavior as often encountered with complex fluids. In addition, a comparison between the surface tension concept and the yield stress concept allowed to explain the relationship between cell invasiveness and yield stress (or surface tension) described in [42], i.e., the smaller the adhesion between cells, the smaller the yield stress the more invasive is the cell clone.

The theoretical basis of this work are the yield stress exhibited by cell suspensions (at a continuum level) and the energy needed to break the adhesion bonds of a cell on an aggregate (at a cell level). On the basis of this experimental evidence, in this paper we have conjectured that also cell aggregates can exhibit a yield adhesion reflecting itself, at a continuum level, in a threshold tension separating an elastic and a viscous regime. The comparison with the very few experiments on cell aggregates present in the literature suggests that this volumetric theory could provide an explanation to the ability of cell aggregates to carry loadsi, alternative to surface tension. Even more important, the re-organization process could explain the permanent strain exhibited by spheroid samples after load.

Of course, the model can and need to be improved in several directions in order to reproduce more closely the behavior of cell aggregates. For instance, one should take into account the fact that the cell aggregate is a porous material filled with the liquid in which the experiment is done. Such an effect can be easily included by adding a further viscous component to the mechanical behavior of the cellular constituent. This is particularly important to explain creeping phenomena occurring when external stresses applied on the cellular aggregate are suddenly applied or released.

Another extension can be represented by the inclusion of more cell re-arrangement times, that can be related to different adhesion mechanisms. These can be due not only to different types of adhesion molecules at the cell membranes but also to the response occurring inside the cell itself with the rearrangement of the adhesion bonds connected to the actin cytoskeleton. In this case also the active role of myosin should be taken into account as well. In addition, more experiments need to be done to understand the origin of the exponent α either using different types of cells, or interphering with the adhesion mechanisms, and to find its dependence on cell concentration.

Deducing a model with more relaxation times would probably lead to a better fit of the experiments by [11, 13, 12, 14]. Nevertheless, the model provided here is a three-dimensional one, different from previous studies [11] suggesting to use simple one–dimensional Maxwell assemblies, coupled with the presence of an arbitrary surface tension. Here we provide a complete description of this visco-elasto-plastic model, and possible parameters have been chosen based on experimental data [20], this leading to relaxation constants in the range of the ones obtained previously [11].

Appendix

In this appendix we will briefly discuss some aspects of kinematics that are useful to deduce the constitutive equation proposed in Section 2. In doing that, one needs to compute the time derivative of the elastic constitutive model

$$\mathbb{T}' = \mu \left(\mathbb{B}_n - \frac{1}{3}\mathrm{tr}\mathbb{B}_n \mathbb{I} \right) , \tag{5.1}$$

which implies to compute the time derivative of $\mathbb{B}_n = \mathbb{F}_n \mathbb{F}_n^T$. This gives

$$\dot{\mathbb{B}}_n = \mathbb{L}_n \mathbb{B}_n + \mathbb{B}_n \mathbb{L}_n^T , \tag{5.2}$$

where

$$\mathbb{L}_n = \dot{\mathbb{F}}_n \mathbb{F}_n^{-1} . \tag{5.3}$$

In the following we will also use the following tensors

$$\mathbb{L} = \dot{\mathbb{F}}\mathbb{F}^{-1} \quad \text{and} \qquad \mathbb{L}_p = \dot{\mathbb{F}}_p \mathbb{F}_p^{-1} . \tag{5.4}$$

Deriving $\mathbb{F}$ in time, one has

$$\dot{\mathbb{F}} = \dot{\mathbb{F}}_n \mathbb{F}_p + \mathbb{F}_n \dot{\mathbb{F}}_p = \mathbb{L}_n \mathbb{F}_n \mathbb{F}_p + \mathbb{F}_n \dot{\mathbb{F}}_p \mathbb{F}_p^{-1} \mathbb{F}_n^{-1} \mathbb{F}_n \mathbb{F}_p = (\mathbb{L}_n + \mathbb{F}_n \mathbb{L}_p \mathbb{F}_n^{-1}) \mathbb{F} , \tag{5.5}$$

that, using the definition (5.4) can be rewritten as

$$\mathbb{L}_n = \mathbb{L} - \mathbb{F}_n \mathbb{L}_p \mathbb{F}_n^{-1} \,. \tag{5.6}$$

Back substitution of (5.6) into (5.2) gives

$$\dot{\mathbb{B}}_n = \mathbb{L}\mathbb{B}_n + \mathbb{B}_n \mathbb{L}^T - 2\mathbb{F}_n \mathbb{D}_p \mathbb{F}_n^T \,, \tag{5.7}$$

where

$$\mathbb{D}_p = \frac{1}{2}(\mathbb{L}_p + \mathbb{L}_p^T) \,, \tag{5.8}$$

or

$$\frac{\mathcal{D}\mathbb{B}_n}{\mathcal{D}t} = -2\mathbb{F}_n \mathbb{D}_p \mathbb{F}_n^T \,, \tag{5.9}$$

where $\mathcal{D}\mathbb{M}/\mathcal{D}t$ is the Maxwell upper convected derivative (2.14).

In this way, we related the evolution of $\mathbb{T}'$ to the evolution of $\mathbb{B}_n$ and through $\mathbb{D}_p$ to the evolution of the natural configuration. On the other hand, in Section 2 we also introduced the equation governing the evolution of the natural configuration

$$\mathbb{F}_n \mathbb{D}_p \mathbb{F}_n^{-1} = \frac{1}{2\tilde{\eta}} \left[1 - \frac{1}{\tilde{f}(\mathbb{T}')} \right]_+ \mathbb{T}' \,, \tag{5.10}$$

where $[\cdot]_+$ stands for the positive part of the argument.

Notice that, coherently with the fact that the l.h.s. of (5.10) is traceless as $\mathbb{T}'$

$$\mathrm{tr}(\mathbb{F}_n \mathbb{D}_p \mathbb{F}_n^{-1}) = \mathrm{tr}\, \mathbb{D}_p = 0 \,. \tag{5.11}$$

In fact, the assumption that the volume ratios in the natural and in the original reference configuration are the same implies $J_p \equiv \det \mathbb{F}_p = 1$. Therefore, from standard tensor calculus, one has

$$\dot{J}_p = J_p \mathrm{tr}\ \mathbb{D}_p = 0 \,, \tag{5.12}$$

which means that $\mathbb{D}_p$ is traceless.

We conclude this appendix by observing that one can re-write (5.10) as

$$\left[1 - \frac{1}{\tilde{f}\left(\frac{\mathbb{S}'_n \mathbb{C}_n}{J_n} \right)} \right]_+ \frac{\mathbb{S}'_n \mathbb{C}_n}{J_n} = 2\tilde{\eta} \mathbb{D}_p \,, \tag{5.13}$$

where $\mathbb{S}'_n = J_n \mathbb{F}_n^{-1} \mathbb{T}' \mathbb{F}_n^{-T}$ is the (excess) second Piola-Kirchhoff stress tensor and $\mathbb{C}_n = \mathbb{F}_n^T \mathbb{F}_n$. It can be noticed that since

$$\mathrm{tr}(\mathbb{S}'_n \mathbb{C}_n) = \mathrm{tr}(J_n \mathbb{F}_n^{-1} \mathbb{T}' \mathbb{F}_n) = J_n \mathrm{tr}\mathbb{T}' = 0 \tag{5.14}$$

$\mathbb{S}'_n \mathbb{C}_n$ is traceless as $\mathbb{D}_p$.

In addition, if we assume that the cellular spheroid obeys a neo-Hookean law,

$$\mathbb{T} = \mu(\phi)(-\Sigma \mathbb{I} + \mathbb{B}_n) \tag{5.15}$$

where $\Sigma = \Sigma(\phi/\phi_n)$, with $\Sigma(1) = 1$, then $\frac{\mathbb{S}'_n \mathbb{C}_n}{J_n}$ has the same eigenvalues as $\mathbb{T}'$ so that $f\left(\frac{\mathbb{S}'_n \mathbb{C}_n}{J_n} \right) = f(\mathbb{T}')$, and $\mu(\phi)$ is the shear elastic modulus.

References

[1] D. Ambrosi and F. Mollica. On the mechanics of a growing tumour. *Int. J. Engng. Sci.*, 40:1297–1316, 2002.

[2] D. Ambrosi and L. Preziosi. Cell adhesion mechanisms and stress relaxation in the mechanics of tumours. *Biomech. Model. Mechanobiol.*, in press, 2009.

[3] I. V. Basov and V. V. Shelukhin. Generalized solutions to the equations of compressible bingham flows. *Z. Angew. Math. Mech.*, 79:185–192, 1999.

[4] G. I. Bell, M. Dembo, and P. Bongrand. Cell adhesion. competition between nonspecific repulsion and specific bonding. *Biophys. J.*, 45(6):1051–1064, 1984.

[5] D. A. Beysens, G. Forgacs, and J. A. Glazier. Cell sorting is analogous to phase ordering in fluids. *Proc. Natl. Acad. Sci. USA*, 97(17):9467–9471, 2000.

[6] R. B. Bird, R. C. Armstrong, and O. Hassager. *Dynamics of polymeric liquids. Volume 1. Fluid mechanics (2nd edition)*. John Wiley and sons, 1987.

[7] R. Buscall, P. D. A. Mills, J. W. Goodwin, and D. W. Lawson. Scaling behaviour of the rheology of aggregate networks formed from colloidal particles. *J. Chem. Soc. Faraday Trans.*, 84:4249–4260, 1988.

[8] S. Chien, S. Usami, R. J. Dellenback, and M. I. Gregersen. Blood viscosity: influence of erythrocyte deformation. *Science*, 157:827–829, 1967.

[9] S. Chien, S. Usami, R. J. Dellenback, M. I. Gregersen, L. B. Nanninga, and M. Mason-Guest. Blood viscosity: influence of erythrocyte aggregation. *Science*, 157:829–831, 1967.

[10] S. Chien, S. Usami, H. M. Taylor, J. L. Lundberg, and M. I. Gregersen. Effects of hematocrit and plasma proteins on human blood rheology at low shear rates. *J. Appl. Physiology*, 21:81–87, 1966.

[11] G. Forgacs, R. A. Foty, Y. Shafrir, and M. S. Steinberg. Viscoelastic properties of living embryonic tissues: a quantitative study. *Biophys. J.*, 74(5):2227–2234, 1998.

[12] R. A. Foty, G. Forgacs, Pfleger, and M. S. Steinberg. Surface tensions of embryonic tissues predict their mutual envelopment behavior. *Development*, 122:1611–1620, 1996.

[13] R. A. Foty, G. Forgacs, C. M. Pfleger, and M. S. Steinberg. Liquid properties of embryonic tissues: Measurement of interfacial tensions. *Phys. Rev. Letters*, 72(14):2298–2301, 1994.

[14] R. A. Foty and M. S. Steinberg. The differential adhesion hypothesis: a direct evaluation. *Dev. Biol.*, 278(1):255–263, 2005.

[15] S. J. Franks, H. M. Byrne, J. R. King, J. C. E. Underwood, and C. E. Lewis. Modelling the early growth of ductal carcinoma in situ of the breast. *J. Math. Biol.*, 47:424–452, 2003.

[16] S. J. Franks, H. M. Byrne, H. S. Mudhar, J. C. E. Underwood, and C.E. Lewis. Mathematical modelling of comedo ductal carcinoma in situ of the breast. *Math. Med. Biol.*, 20:277–308, 2003.

[17] Y. C. Fung. Microrheology and constitutive equation of soft tissue. *Biorheology*, 25:261–270, 1978.

[18] R. F. Gibson. *Principles of Composite Material Mechanics*. Mc Graw-Hill, 1994.

[19] K. Hyun, S. H. Kim, K. H. Ahn, and S. J. Lee. Large amplitude oscillatory shear as a way to classify the complex fluids. *J. Non-Newtonian Fluid Mech.*, 107:51–65, 2002.

[20] A. Iordan, A. Duperray, and C. Verdier. Fractal approach to the rheology of concentrated cell suspensions. *Phys. Rev. E*, 77(1):011911, 2008.

[21] D. D. Joseph. *Fluid Dynamics of Viscoelastic Liquids*. Springer, 1990.

[22] E. Kroener. Allgemeine kontinuumstheorie der versetzungen und eigenspannungen. *Arch. Rational Mech. Anal.*, 4:273–334, 1960.

[23] E. Lee. Elastic-plastic deformation at high strains. *J. Applied Mechanics*, 36:1–6, 1969.

[24] W. A. Malik, S. C. Prasad, K. R. Rajagopal, and L. Preziosi. On the modelling of the viscoelastic response of embryonic tissues. *Math. Mech. Solids*, 13:81–91, 2008.

[25] L. E. Malvern. *Introduction of the Mechanics of a Continuous Medium*. Prentice Hall Inc., 1969.

[26] J. C. M. Mombach and J. A. Glazier. Single cell motion in aggregates of embryonic cells. *Phys. Rev. Letters*, 76:3032–3035, 1996.

[27] J. C. M. Mombach, D. Robert, F. Graner, G. Gillet, G. L. Thomas, M. Idiart, and J. P. Rieu. Rounding of aggregates of biological cells: Experiments and simulations. *Physica A*, 352:525–534, 2005.

[28] H. M. Phillips and M. S. Steinberg. Embryonic tissues as elasticoviscous liquids. i. rapid and slow shape changes in centrifuged cell aggregates. *J. Cell. Sci.*, 30:1–20, 1978.

[29] H. M. Phillips, M. S. Steinberg, and B. H. Lipton. Embryonic tissues as elasticoviscous liquids. ii. direct evidence for cell slippage in centrifuged aggregates. *Develop. Biol.*, 59:124–134, 1977.

[30] L. Preziosi. On an invariance property of the solution to stokes' first problem for viscoelastic fluids. *J. Non-Newtonian Fluid Mech.*, 33:225–228, 1989.

[31] L. Preziosi and D. D. Joseph. Stokes' first problem for viscoelastic fluids. *J. Non-Newtonian Fluid Mech.*, 25:239–259, 1987.

[32] S. Reynaert, P. Moldenaers, and J. Vermant. Interfacial rheology of stable and weakly aggregated two-dimensional suspensions. *Phys. Chem. Chem. Phys.*, 9:6463–6475, 2007.

[33] J. P. Rieu, K. Tsuchiya, S. Sawai, Y. Maeda, and Y. Sawada. Cell movements and traction forces during the migration of 2-dimensional dictyostelium slugs. *J. Biol. Phys.*, 29:1–4, 2003.

[34] J. P. Rieu, A. Upadhyaya, J. A. Glazier, N. B. Ouchi, and Y. Sawada. Diffusion and deformations of single hydra cells in cellular aggregates. *Biophys. J.*, 79:1903–1914, 2000.

[35] P. Saramito. A new constitutive equation for elastoviscoplastic fluid flows. *J. Non-Newtonian Fluid Mech.*, 145:1–14, 2007.

[36] P. Saramito. A new elastoviscoplastic model based on the herschel-bulkley viscoplasticity. *J. Non-Newtonian Fluid Mech.*, 158:154–161, 2009.

[37] P. Snabre, M. Bitbol, and P. Mills. Cell disaggregation behavior in shear flow. *Biophys. J.*, 51(5):795–807, 1987.

[38] P. Snabre and P. Mills. I. rheology of weakly flocculated suspensions of rigid particles. *J. Phys. III. France*, 6:1811–1834, 1996.

[39] W. Supatto, D. Débarre, B. Moulia, E. Brouzés, J.L. Martin, E. Farge, and E. Beaurepaire. In vivo modulation of morphogenetic movements in drosophila embryos with femtosecond laser pulses. *Proc. Natl. Acad. Sci. USA*, 102(4):1047–1052, 2005.

[40] G. B. Thurston. Viscoelasticity of human blood. *Biophys. J.*, 12:1205–1217, 1972.

[41] C. Verdier. Review. rheological properties of living materials: From cells to tissues. *J. Theor. Med.*, 5(2):67–91, 2003.

[42] B. S. Winters, S. R. Shepard, and R. A. Foty. Biophysical measurement of brain tumor cohesion. *Int. J. Cancer*, 114(3):371–379, 2005.